Ion implantation of silicon at the nanometer scale

Marco Bianconi[a] and Fabio Bergamini
CNR-IMM-Sezione di Bologna, Via P. Gobetti 101, I-40129 Bologna, Italy and Laboratory MIST E-R, Via P. Gobetti 101, I-40129 Bologna, Italy

Stefano Cristiani and Giorgio Lulli
CNR-IMM-Sezione di Bologna, Via P. Gobetti 101, I-40129 Bologna, Italy

(Received 18 July 2007; accepted 8 August 2007; published online 4 October 2007)

SiO_2 layers (~0.5 μm thick) thermally grown on (100) Si were irradiated with 12.5 MeV Ti ions at 10^9 cm^{-2} fluence, and subsequently exposed to the HF vapor, in order to selectively etch the latent tracks generated by the passage of swift ions. Nearly cylindrical nanoholes having diameters as small as 25 nm, with an average value of 54±5 nm, were generated by this procedure. The nanopatterned SiO_2 layer served as a mask for selective amorphization of the underlying Si, achieved by implantation with 180 keV Ar^+ ions at a fluence of 2.0×10^{15} cm^{-2}. Dip in aqueous HF solution was then performed to selectively etch ion amorphized Si, thus transferring the nanometric pattern of the SiO_2 mask to the underlying substrate. As expected, the maximum depth of amorphizazion in Si, and consequently of etching depth, decreases when the hole radius decreases below values of the order of the lateral ion straggling. The effect has been characterized and investigated by the comparison of experiments and three dimensional Monte Carlo simulations.
 [DOI: 10.1063/1.2786098]

I. INTRODUCTION

The modification of the structural and chemical properties of solids by ion implantation is a well consolidated topic of material science. The introduction of moderate amounts of damage in the crystalline structure has several applications such as the formation of waveguides in integrated optical devices[1,2] or the lifetime control in high power electronic devices.[3,4] When large concentrations of defects or amorphization are attained, the etching properties of the implanted layers can be considerably modified and both etching enhancement and frustration have been observed in semiconductors and insulators.[5–8] Usually amorphization is achieved by accumulation of defects and/or overlapping of small damaged volumes produced by nuclear interaction of the beam with the target atoms. In the case of insulators, the interaction of swift heavy ions with the electronic system in a localized volume surrounding the ion path gives rise to additional phenomena leading to the formation of latent tracks that can be subsequently etched by using a suitable chemical agent.[9]

In general, the etching ratio of implanted to unimplanted areas can be very high, even orders of magnitude, and this selectivity is suitable for the fabrication of submicrometric surface structures. Although the development of nanotechnology has triggered a renewed interest in this field, relatively few investigations have been devoted to explore the possibility and the limits of ion implantation at the nanometer scale.[10–13] In this paper we investigate this subject both experimentally, using a new method for Silicon machining at the nanometer scale, and theoretically, with three dimensional (3D) Monte Carlo simulation of ion implantation through nanometer apertures.

[a]Electronic mail: bianconi@bo.imm.cnr.it

II. EXPERIMENTAL

Silicon (100) CZ *n*-type 0.5–1 Ω cm wafers were thermally oxidized in wet atmosphere at 920 °C to produce SiO_2 films with a nominal thickness of 460 nm. The wafers were irradiated at normal incidence (0±1° tilt) by 12.5 MeV Ti^{+7} ions at a fluence of $1.0\pm0.2\times10^9$ cm^{-2}. The electronic energy losses are about 420 and 360 eV/Å at the entrance of the SiO_2 layer and the bulk Si, respectively. The samples were cut into 2×2 cm^2 pieces and cleaned in boiling acetone for 5 min, followed by isopropilic alcohol for 5 min, HF(49%):H_2O 1:10 for 5 s, and finally rinsed in de-ionized water. After Ti irradiation, ion track etching was performed by heating the samples at 40 °C and by exposing them to the vapors of a HF(49%):H_2O 1:4 solution at $T=25$ °C for 50 min. The details of this process are described in Ref. 14.

In order to study the usability of the above structure as a mask for nanometer scale ion implantation, the samples were subsequently implanted at normal incidence (0±1° tilt) with 180 keV Ar^+ ions at a fluence of $2.0\pm0.2\times10^{15}$ cm^{-2}. The ion flux was about 7×10^{11} cm^{-2} sec^{-1}. No appreciable deviation from room temperature was measured on the sample holder. During implantation, in the same batch some virgin silicon test samples, partially covered with a metal mask having circular apertures in the 200–500 μm range, were also implanted. Finally the samples were immersed in a HF(49%):H_2O 1:10 quiescent solution at room temperature first for 15 min to remove the oxide layer, and then for different times up to 5 h to etch the damaged silicon.

Some test samples were analyzed by Rutherford backscattering spectrometry in channeling geometry (RBS-C) to determine the damage depth profile. The measurements were performed using a 2 MeV He^+ beam, and a backscattering angle of 170° in the ⟨100⟩ alignment. Details of the measurement setup are reported in Ref. 15. Scanning electron mi-

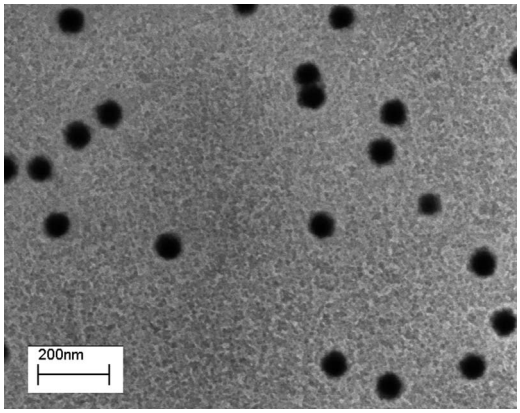

FIG. 1. SEM planar view of the SiO_2 layer after implantation with 12.5 MeV Ti ions and subsequent ion track etching in HF vapor.

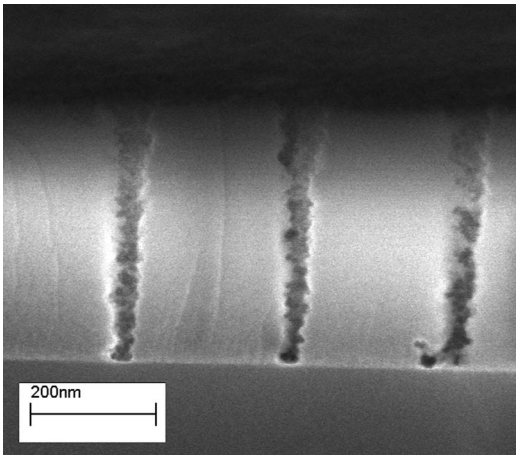

FIG. 2. SEM cross-section view of the sample of Fig. 1.

croscopy (SEM) characterization was performed by a Gemini Leo 1530 microscope by using a gun voltage of 5 kV. Swelling measurements were performed by using a Veeco Dektak 6M mechanical profilometer.

III. MODELING

Implantation through nanoholes was modeled with KING3D, a 3D version of KING, a computer program for the simulation of ion implantation in crystalline Si based on the Monte Carlo binary collision approximation (MC-BCA). Details about the code and the physical models used therein have been reported elsewhere.[16–18] For the purposes of the present work, a fully 3D simulation scheme was developed. Each ion randomly impinges at the surface of a SiO_2/Si structure, where the SiO_2 overlayer is patterned with holes having either cylindrical or truncated conical shape. Small random fluctuations in hole diameter as a function of depth are used to mimic wall roughness. 3D ion penetration and recoil calculation are performed both in the Si substrate and in the SiO_2 mask. This allows us to account for effects, such as transmission through mask, scattering at walls, and injection of recoils from the mask into the Si substrate, which are essential to correctly simulate implantation through apertures of large depth to width ratio. Periodic boundary conditions are applied parallel to the wafer surface. According to this scheme, the ion impact domain represents the unit cell of an infinite periodic pattern. To simulate the case of an isolated hole, the size of the impact region must be larger than the sum of the hole diameter plus twice the maximum radial ion straggling. Distributions of disorder in the Si substrate result from full recoil calculations, where the threshold energy for elastic displacement of Si atoms is assumed to be 13 eV. To ensure good damage statistics the number of primary ions calculated for each run was in the range of $0.8–2\times10^6$, which results in CPU load of 7–15 h on a single node of a 64-bit AMD series 242 dual processor.

IV. RESULTS

The oxide surface after high energy implantation and vapor etching is shown in Fig. 1. Circular etched tracks are clearly visible and their areal density equals the ion fluence ($1.0\pm0.2\times10^9$ cm^{-2} in the present case). A cross-sectional view of the edge of a cleaved sample is showed in Fig. 2. The oxide thickness after etching is 410 ± 10 nm. The nanopore's diameter distribution (measured at half depth in the oxide layer) has a mean value of 54 nm and a standard deviation of 5 nm. Larger, noncircular holes generated by the superposition of two or more tracks are also visible. Due to the stochastic nature of the ion impingement these events are rather frequent. The nanopores have a conical shape, their walls are inclined $\sim2.5°$ to the pore axis and have a roughness of ±5 nm.

Ion implantation through the nanopatterned SiO_2, followed by oxide removal and etching of Si damaged regions below, is a viable way to produce nanoholes in the Si substrate. In general, enhanced etching of Si has been reported as a suitable technique for submicrometric pattern fabrication (see Refs. 19 and 20 and references therein). HF has been proven to be an effective etchant for these applications (considering that crystalline Si is practically insoluble in this acid[21]) even if the nature of the process has not been clearly explained yet. It has been shown[22,23] that the removal of silicon amorphized by ion implantation is grossly nonuniform and that different cooling arrangements and experimental conditions of the implantation step lead to highly variable etching rates. Before implantation through the nanopatterned SiO_2, we implanted reference Si samples partially covered by a metal mask with 180 keV Ar^+ ions at a fluence of $2.0\pm0.2\times10^{15}$ cm^{-2}. In spite of the accurate control of the beam current, we actually observed a remarkable variability in the etching rate of the samples and we believe that the origin of this problem lies in the nonreproducibility of the thermal contact between the mask and the sample. In Fig. 3 we show the evolution of the step height as a function of the etching time in the HF(49%):H_2O 1:10 quiescent solution for one of the samples which exhibited the largest etching rate (~5 nm/min).

The SEM planar view of the Si sample with the nanopatterned SiO_2 overlayer after the same implantation step, followed by 2 h etching in the HF solution, is shown in Fig. 4. The surface is smooth and the features of the oxide masking layer have been transferred to the bulk silicon. The average hole diameter at the surface is 58 ± 10 nm. In Fig. 5 a cross-sectional view of one of these nanoholes is shown. In

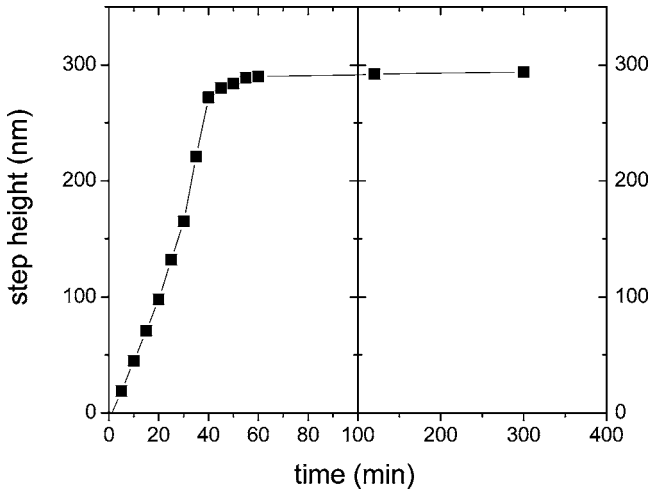

FIG. 3. Stylus profilometer measurement of the step height vs wet etching time for a bulk Si sample implanted with 2×10^{15} cm^{-2}, 180 keV Ar ions at normal incidence.

the case of these samples we found a satisfactory reproducibility in the etching rates. The amorphized regions were always removed in about 1 h, in agreement with the data of Fig. 3, whereas any further immersion in the HF bath (we tried additional times of 3 and 5 h) had no substantial effect on the size of the holes developed in the silicon substrate.

V. CALCULATIONS AND DISCUSSION

We performed RBS channeling analysis of some bulk reference Si samples implanted with 180 keV Ar^+ ions at a fluence of $2.0\pm0.2\times10^{15}$ cm^{-2} and normal incidence. The damage depth profiles were extracted from MC simulation of the experimental spectra by the computer code BISIC.[15,24] The result is showed in Fig. 6. Besides a thin partially damaged surface region a fully disordered (amorphous) layer extends up to a depth of ~280 nm, followed by a deeper tail of damage. We measured a swelling of 6 nm in these samples; considering the thickness of the amorphized region as measured by RBS, this value confirms the ~2% volume increase upon amorphization measured in Ref. 25. The dashed vertical line corresponds to the etch stop depth (see Fig. 3). On the basis of this result, we assume the threshold for the etching of damaged Si at the disorder fraction 0.65 ± 0.05. The maximum etched depth is considerably smaller when the ion implantation is performed through the nanopatterned mask than when is performed though the metal mask, or in the bulk. To investigate this size effect, the implantation process was modeled using the KING3D code, and the result of the simulation of the process corresponding to the case shown in Fig. 5 is reported in Fig. 7. If we assume that etching is effective for damage levels larger than 0.65, the nanohole shape and size foreseen by the simulation are in good agreement with the experimental ones. It was found that the best agreement is achieved when the true conical shape of the SiO_2 apertures (Fig. 2) is taken into account. The reduced amorphization depth, as compared with the macroscopic case, is the result of the limited overlapping of the ion trajectories, which becomes effective when the lateral straggling of ions (~50 nm for 180 keV Ar^+) is comparable to the radius of the mask aperture. The simulation indicates that, with increasing the ion fluence, the amorphization depth should increase. However, preliminary experiments showed us that self-annealing phenomena occur for fluences of the order of 1×10^{16} cm^{-2}, at least for the ion fluxes employed

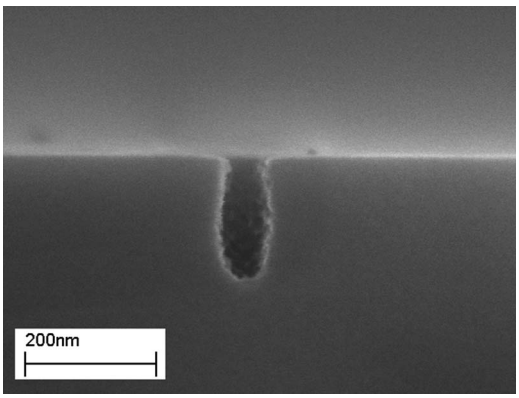

FIG. 5. SEM cross-section view of the sample of Fig. 2.

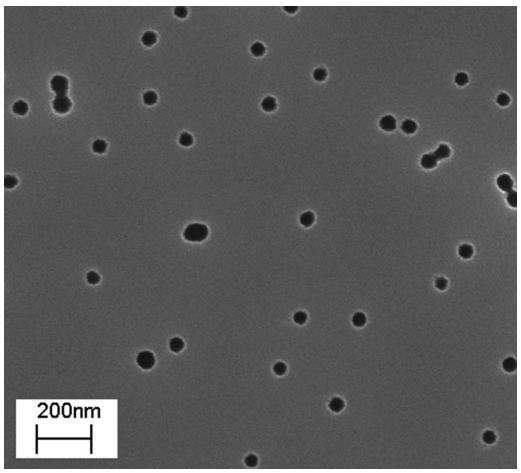

FIG. 4. SEM planar view of a Si sample implanted through the SiO_2 masking layer with 2×10^{15} cm^{-2}, 180 keV Ar ions and subsequently etched in HF(49%):H_2O 1:10 quiescent solution for 2 h.

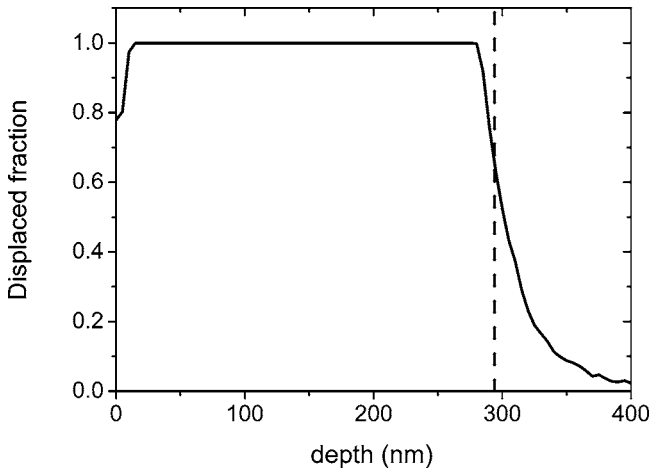

FIG. 6. Damage depth profile measured by RBS channeling for a Si sample implanted with 2×10^{15} cm^{-2}, 180 keV Ar ions at normal incidence. The dashed vertical line indicates the depth of the etch stop for the process shown in Fig. 4.

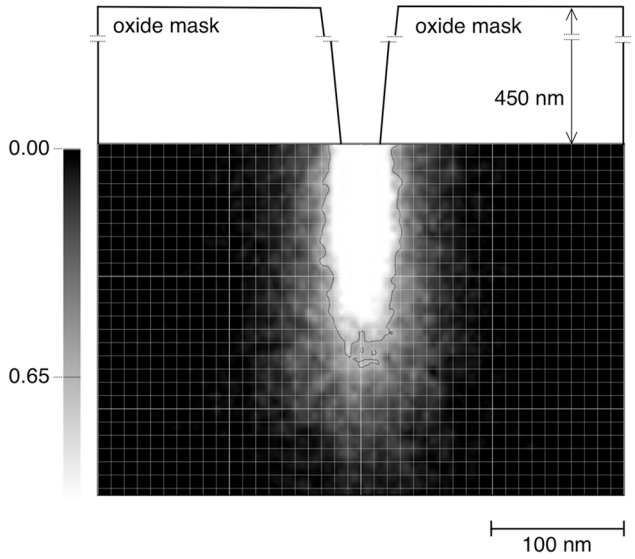

FIG. 7. KING3D simulation of an ion implantation step through the SiO_2 masking layer with 50 nm wide and 450 nm deep nanopores. In agreement with the shape of holes shown in Fig. 1(b), the aperture has the shape of a truncated cone, with a diameter at the SiO_2 surface of ~80 nm and a diameter at the Si surface of 60 nm. The gray scale represents the displaced fraction of Si lattice atoms as a function of the spatial coordinates on a plane sectioning the diameter of the hole.

here and in absence of sample cooling, resulting in a saturation of the damaged fraction at large depth.

Figure 8 (symbols) shows the plot of the experimental maximum etched depth as a function of the surface diameter as obtained by the SEM cross-section observations. We only considered nanoholes having diameter less than 90 nm. As already discussed before, larger diameter holes with noncircular shape are generated by the occasional overlapping of two or more tracks in the oxide mask. The results of the KING3D simulation are plotted in Fig. 8 for comparison. The dashed line was obtained for ideal cylindrical pores in the oxide mask, whereas the solid line was obtained for conical pores having the shape as determined by SEM. The uncertainty in the simulated maximum depth is 20 nm. Mask size

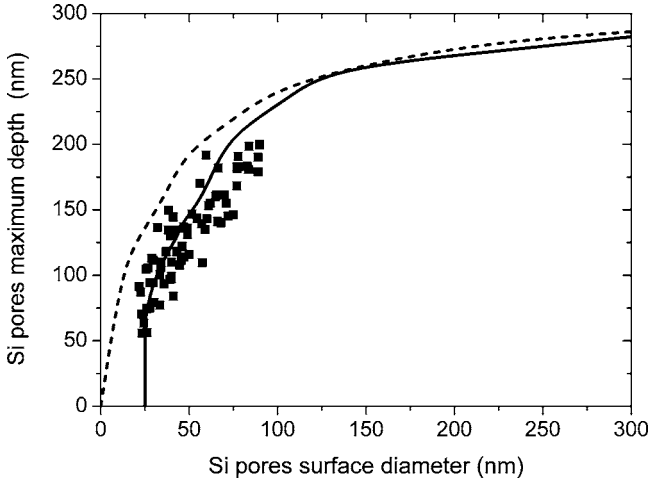

FIG. 8. Plot of the maximum etched depth of implanted Si as a function of the surface diameter. Experimental data (symbols), simulation with ideal cylindrical pores (dashed line), and conical pores (solid line) in the oxide mask.

effects already occur for hole diameters of 200–300 nm and become critical when the mask size is comparable with the ion lateral straggling. The agreement with experiment is good. The effect of conicity is to limit the minimum transferable diameter that, in present case, amounts to about 25 nm; a mask having ideal vertical walls seems then necessary to obtain smaller features. Simulations were also performed by introducing a ripple of ±5 nm in the mask wall diameter to mimic the observed wall roughness; the difference with the case of smooth walls was found to be negligible.

VI. CONCLUSIONS

Circular holes having diameters as small as 25 nm have been obtained on the surface of crystalline Si wafers by etching selected regions amorphized by ion implantation through a nanostructured SiO_2 mask produced by ion track technology. The amorphized depth is smaller than the one obtained for implantation through micrometer sized apertures. This size effects, characterized by 3D MC-BCA simulation, becomes effective when the mask aperture size is comparable with the ion lateral straggling. Simulation is in good agreement with experiment, provided that the true conical shape of nanoholes in the SiO_2 mask is taken into account. Conicity limits the minimum transferable diameter to ~25 nm. The simulation indicates that vertical pore walls are required to obtain smaller features.

[1]P. D. Townsend, Nucl. Instrum. Methods Phys. Res. B **65**, 243 (1992).
[2]P. D. Townsend, J. Phys. E **10**, 197 (1977).
[3]P. Hazdra, J. Vobecky, and K. Brand, Nucl. Instrum. Methods Phys. Res. B **186**, 414 (2002).
[4]P. Cova, R. Menozzi, M. Portesine, M. Bianconi, E. Gombia, and R. Mosca, Solid-State Electron. **49**, 183 (2005).
[5]J. F. Gibbons, E. O. Hecht, and T. Tsurushima, Appl. Phys. Lett. **15**, 117 (1969).
[6]M. Masahara, Y. X. Liu, S. Hosokawa, T. Matsukawa, K. Ishii, H. Tanoue, K. Sakamoto, T. Sekigawa, H. Yamauchi, S. Kanemaru, and E. Suzuki, IEEE Trans. Electron Devices **51**, 2078 (2004).
[7]P. Levy, M. Bianconi, and L. Correra, J. Electrochem. Soc. **145**, 344 (1998).
[8]M. Koh, T. Goto, A. Sugita, T. Tanii, T. Iida, T. Shinada, T. Matsukawa, and I. Ohdomari, Jpn. J. Appl. Phys., Part 1 **40**, 2837 (2001).
[9]M. Toulemonde, C. Trautmann, E. Balanzat, K. Hjort, and A. Weidinger, Nucl. Instrum. Methods Phys. Res. B **216**, 1 (2004).
[10]N. Matsuura, T. W. Simpson, I. Mitchell, X. Y. Mei, P. Morales, and H. E. Ruda, Appl. Phys. Lett. **81**, 4826 (2002).
[11]L. E. Rehn, B. J. Kestel, P. M. Baldo, J. Hiller, A. W. McCormick, and R. C. Birtcher, Nucl. Instrum. Methods Phys. Res. B **206**, 490 (2003).
[12]A. Razpet, A. Johansson, G. Possnert, M. Skupiński, K. Hjort, and A. Hallen, J. Appl. Phys. **97**, 044310 (2005).
[13]M. L. Taylor, R. D. Franich, A. Alves, P. Reichart, D. N. Jamieson, and P. N. Johnston, Nucl. Instrum. Methods Phys. Res. B **249**, 752 (2006).
[14]F. Bergamini, M. Bianconi, and S. Cristiani, Nucl. Instrum. Methods Phys. Res. B **257**, 593 (2007).
[15]G. Lulli, E. Albertazzi, M. Bianconi, G. G. Bentini, R. Nipoti, and R. Lotti, Nucl. Instrum. Methods Phys. Res. B **170**, 1 (2000).
[16]E. Albertazzi, M. Bianconi, G. Lulli, R. Nipoti, A. Carnera, and C. Cellini, Nucl. Instrum. Methods Phys. Res. B **112**, 152 (1996).
[17]G. Lulli, M. Bianconi, R. Nipoti, E. Albertazzi, M. Cervera, A. Carnera, and C. Cellini, J. Appl. Phys. **82**, 5958 (1997).
[18]The executable of the one dimensional version of KING program (running on i386 linux platform) can be downloaded at http://lotto.bo.imm.cnr.it/research/ionimpl/openking_page.html
[19]K. Moriwaki, N. Masuda, H. Aritome, and S. Namba, Jpn. J. Appl. Phys. **19**, 491 (1980).

[20]K. Moriwaki, H. Aritome, and S. Namba, Jpn. J. Appl. Phys. **20**, 1305 (1981).
[21]G. Willeke and K. Kellermann, Semicond. Sci. Technol. **11**, 415 (1996).
[22]L. Liou, W. G. Spitzer, and S. Prussin, J. Electrochem. Soc. **131**, 672 (1984).
[23]K. N. Tu, S. I. Tan, and B. L. Crowder, Appl. Phys. Lett. **22**, 274 (1973).
[24]E. Albertazzi, M. Bianconi, G. Lulli, R. Nipoti, and M. Cantiano, Nucl. Instrum. Methods Phys. Res. B **118**, 128 (1996).
[25]G. Lulli, E. Albertazzi, M. Bianconi, R. Nipoti, M. Cervera, A. Carnera, and C. Cellini, J. Appl. Phys. **82**, 5958 (1997).